Dynamics of the RNA Hairpin GNRA Tetraloop†

Marcus Menger,‡ Fritz Eckstein,§ and Dietmar Porschke*,‡

Max-Planck-Institut für biophysikalische Chemie, D-37077 Göttingen, Germany, and Max-Planck-Institut für experimentelle Medizin, D-37075 Göttingen, Germany

Received October 4, 1999

ABSTRACT: The dynamics of RNA hairpin tetraloops of the GNRA type [sequence G- any ribonucleotide (N)-purine (R)-A] was analyzed by fluorescence spectroscopy and by fluorescence-detected temperature-jump relaxation, using RNA oligomers with 2-aminopurine (2AP) substituted in two different positions of the loop sequence, Gp2APpApA (HP1) and GpAp2APpA (HP2), as indicator. The fluorescence of HP1 is much higher than that of HP2, indicating a lower degree of 2AP-stacking in HP1. Addition of Mg^{2+} or Ca^{2+} ions leads to an increase of fluorescence in HP1, whereas a decrease of fluorescence is observed in HP2. In both cases at least two ion-binding equilibria are required to fit titration data. T-jump experiments using fluorescence detection show a relaxation process with a time constant of 22 μs for HP1, whereas two relaxation processes with time constants 5 and 41 μs, are found for HP2. These results clearly demonstrate the existence of more than the single conformation state detected by NMR analysis. The T-jump amplitudes decrease with increasing bivalent ion concentration, indicating that one of the states is favored in the presence of bivalent ions. The loop relaxation processes are slower than standard stacking processes, probably because of activation barriers imposed by a restricted mobility of loop residues, and are assigned to a stacking rearrangement, probably between the 5′ and the 3′-side. A similar process has been observed previously for the anticodon loop of $tRNA^{Phe}$. The rate constants of the transition are in the range of 10^4 s^{-1} in the case of HP1. The data demonstrate the existence of structures that are not resolved by standard NMR because of fast exchange and are not found by X-ray analysis because of restrictions by crystal packing.

Hairpins with tetraloops of the GNRA family [sequence G- any ribonucleotide (N)-purine (R)-A] are abundant structure elements in natural RNAs. These hairpins are particularly stable and are often involved in tertiary contacts (*1*). It is likely that these hairpin loops are important nucleation sites to ensure proper folding of large RNA structures. Various members of the tetraloop family have been investigated by computer modeling (*2*, *3*) and NMR structure analysis (*4*−*7*). Structures of tetraloops were also determined by X-ray analysis in hammerhead ribozymes (*8*, *9*), in a group I ribozyme (*10*, *11*), and in a fragment of 5S RNA (*12*). Various spectroscopic techniques have been used to characterize tetraloops, for example Raman and CD spectroscopy (*13*, *14*). The results of these investigations provide well-defined structures and detailed descriptions of the interactions.

The dynamics of tetraloop structures has been studied by computer simulations (*15*). Motions of loop residues on the time scale of pico- to nanoseconds were analyzed by ^{15}N spin relaxation (*16*). The interconversion between hairpin and duplex forms has also been studied (*17*, *18*). In the present investigation the dynamics of GNRA tetraloops is analyzed by fluorescence-detected temperature-jump relaxation using loops with 2-aminopurine substitution. Relaxation effects in the time range from 5 to 100 μs demonstrate the existence of more than a single conformation state. These states are hard to detect by conventional NMR techniques, because of their high interconversion rates beyond the fast exchange limit.

MATERIALS AND METHODS

The hairpin loop structures (Figure 1) $A(pA)_6$ p(2AP)-$(pA)_4$ [2AP-oligo(A)] and $A(pA)_5$ pGp(2AP)$(pA)_4$ were synthesized by the solid-phase method and purified as previously described (*19*, *20*).

For most of the measurements a standard buffer B containing 0.1 M $NaClO_4$ and 50 mM cacodylic acid/Tris, pH 7.2, was used. Some measurements were conducted in a buffer T containing 75 mM Tris-HCl, pH 7.5, and in a low-salt buffer C, containing 1 mM sodium cacodylate, pH 7.0.

Fluorescence intensities were measured with an SLM 8000 spectrofluorometer, interfaced to a PC for data collection and averaging. The fluorescence was excited at 320 nm with a bandwidth of 1 nm; the emission was measured at 380 nm with a bandwidth of 16 nm. Before measurements, all solutions were centrifuged within the cuvette in a low-speed desk-top centrifuge for 2 min to clear the solution of dust particles. After thermostating in the cuvette holder for 5 min, the fluorescence intensity was measured for 400 s. There

† This work was supported by grants to F.E. and D.P. from the Deutsche Forschungsgemeinschaft. The facilities of the Gesellschaft für wissenschaftliche Datenverarbeitung mbH, Göttingen, were used for data processing.

* To whom correspondence should be addressed: Fax (49) 551−2011168; E-mail dpoersc@gwdg.de.

‡ Max-Planck-Institut für biophysikalische Chemie.

§ Max-Planck-Institut für experimentelle Medizin.

10.1021/bi992297n CCC: $19.00
Published on Web 03/22/2000

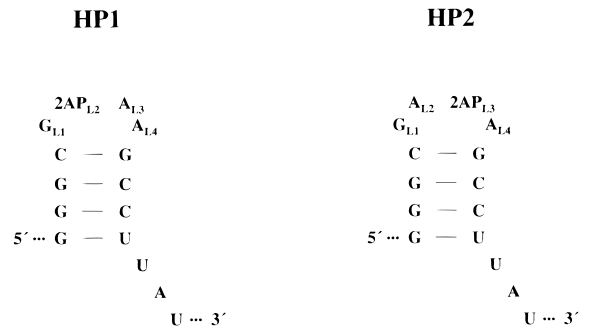

FIGURE 1: Sequence and secondary structure of the hairpin loops HP1 and HP2.

was no indication of a slow process under these conditions. After correction by reference measurements, the data were fitted by least-squares fitting routines using the facilities of the Gesellschaft für wissenschaftliche Datenverarbeitung mbH, Göttingen. The model used for fitting of the titration data is described by Menger et al. (*20*).

UV melting curves were determined by a Cary 219 spectrophotometer interfaced to a PC and a Haake F3C thermostat together with a PG20 programming device. Melting temperatures T_m and ΔH values were evaluated as described by Porschke and Jung (*21*).

Temperature jump relaxation was measured with an instrument of the type described by Rigler et al. (*22*) with improvements by Rabl (unpublished results). A 200 W Xe/Hg arc lamp together with a Schoeffel GM250 monochromator was used as light source. The fluorescence was excited at 313 nm and collected behind cutoff filters GG385 (2 mm) from Schott (Mainz). The transients were initially stored on a Biomation 1010 waveform recorder and finally transmitted to the facilities of the Gesellschaft für wissenschaftliche Datenverarbeitung mbH, Göttingen, for exponential fitting by deconvolution procedures according to either Porschke and Jung (*23*) or Diekmann et al. (*24*).

The concentration dependence of relaxation time constants and amplitudes was simulated for given reaction models by the program SIMULA (*25*; modified by R. Clegg, J. Reiter, and M. Jung, private communication). The data obtained for the hairpin loop HP1 were also fitted by a least-squares fitting procedure with an independent algorithm based on a procedure described by Ilgenfritz (*26*); the resulting parameters were equivalent within the limits of accuracy.

RESULTS

Equilibrium Parameters. The hairpin loops used in the present investigation contain a fluorescent nucleotide which may induce some change of the structure and the stability of the loop. A simple test for any change of the loop was performed by an analysis of the parameters of the thermal helix-coil transition. Because of the high T_m values in the standard buffer, we used the low-salt buffer C for melting experiments and found cooperative transitions in absorbance−temperature profiles with T_m values 67 ± 1 °C for HP1 and 65 ± 1 °C for HP2. ΔH values derived by application of the van't Hoff equation are 37 ± 2 kcal/mol both for HP1 and HP2. These values are quite close to those found for a hairpin without 2-aminopurine substitution (T_m = 70 ± 1 °C, ΔH = 33 ± 2 kcal/mol) and, thus, indicate that substitution with 2-aminopurine does not induce any substantial change in the hairpin loop structure.

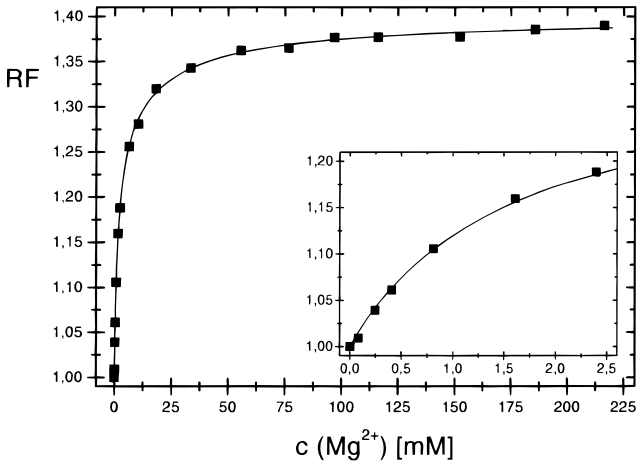

FIGURE 2: Relative fluorescence intensity of HP1 as a function of the Mg^{2+} concentration in buffer B at 20 °C. The inset shows the data at low Mg^{2+} concentrations. The line represents a least-squares fit for two independent binding sites with binding constants 674 M^{-1} and 48 M^{-1} and relative quantum yields 1.29 and 1.07, respectively.

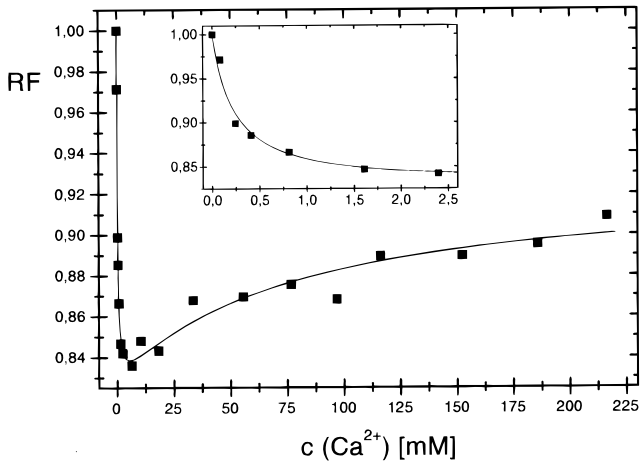

FIGURE 3: Relative fluorescence intensity of HP2 as a function of the Ca^{2+} concentration in buffer T at 20 °C. The inset shows the data at low Ca^{2+} concentrations. The line represents a least-squares fit for two independent binding sites with binding constants 4340 M^{-1} and 14 M^{-1} and relative quantum yields 0.82 and 1.15, respectively.

As first described by Ward et al. (*27*), the fluorescence of 2-aminopurine is decreased when it is involved in stacking interactions in oligo- or polynucleotides. Thus, the relative fluorescence intensity can be used as indicator of the degree of stacking. The fluorescence of 2-aminopurine in HP1 is 16% ± 1% of that found for free 2-aminopurine ribonucleoside, whereas the corresponding fluorescence level in HP2 is only 1.8% ± 0.2% (20 °C, buffer B). Because 2-aminopurine is next to a guanine in HP1 and guanine is known to quench fluorescence (*28*), we compared the fluorescence intensities of the single-stranded oligoribonucleotides $A(pA)_6$ $p(2AP)(pA)_4$ and $A(pA)_5$ $pGp(2AP)(pA)_4$. We found that the A → G replacement induced a decrease of the fluorescence intensity by a factor of 1.9. Thus, this decrease cannot explain the difference of fluorescence intensities for HP1 and HP2, which must mainly be due to a difference in the degree of 2-aminopurine stacking. Although the fluorescence intensity

Table 1: Results Obtained from Fluorescence Titrations[a]

RNA	Me^{2+} ion	buffer	ΔRF (%)	K_1 (M^{-1})	K_2 (M^{-1})	$q1$	$q2$
HP1	Mg	B	+(41 ± 2)	820 ± 160	40 ± 8	1.29 ± 0.01	1.08 ± 0.01
	Ca	B	+(41 ± 2)	660 ± 150	26 ± 15	1.31 ± 0.01	1.07 ± 0.01
	Mg	T	+(51 ± 3)	2460 ± 100	83 ± 34	1.35 ± 0.02	1.09 ± 0.01
	Ca	T	+(48 ± 2)	2570 ± 100	97 ± 30	1.32 ± 0.02	1.09 ± 0.01
HP2	Mg	B	−(10 ± 3)	690 ± 380	53 ± 40	0.79 ± 0.09	1.26 ± 0.18
	Ca	B	−(11 ± 1)	810 ± 370	36 ± 53	0.79 ± 0.11	1.23 ± 0.29
	Mg	T	−(20 ± 5)	4770 ± 200	49 ± 40	0.77 ± 0.02	1.06 ± 0.02
	Ca	T	−(9 ± 3)	4340 ± 200	14 ± 35	0.82 ± 0.02	1.15 ± 0.02

[a] ΔRF is the relative change of fluorescence; $q1$ and $q2$ are the quantum yields of the first and the second complex relative to that of the free hairpin. The bivalent ions were added up to concentrations of 220 mM.

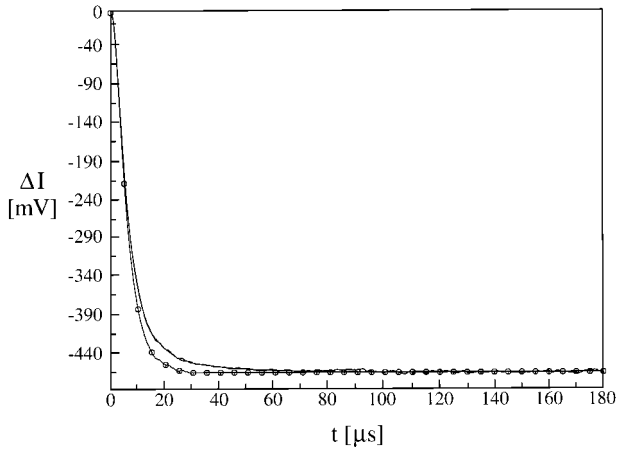

FIGURE 4: Temperature-jump relaxation of HP1 detected by fluorescence induced by a temperature jump from 2 to 8.1 °C (buffer B, 7.1 μM HP1). The line marked with circles represents the reference for deconvolution. The exponential fit (τ^c = 22.1 μs) cannot be distinguished from the experimental data.

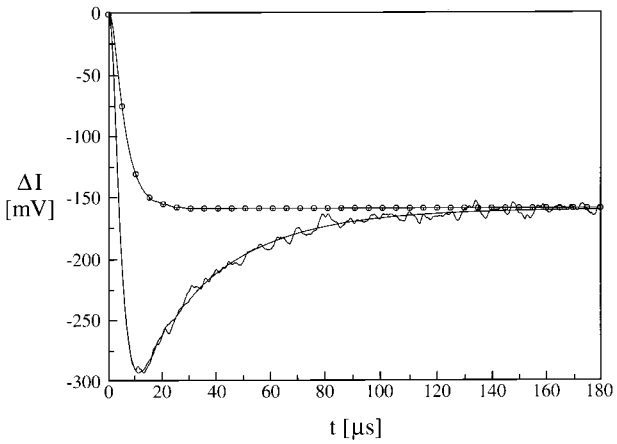

FIGURE 5: Temperature-jump relaxation of HP2 detected by fluorescence induced by a temperature jump from 2 to 8.1 °C (buffer B, 7.1 μM HP2). The line marked with circles represents the reference for deconvolution. The exponential fit (τ^c_1 = 5.2 μs, τ^c_2 = 41.3 μs) cannot be distinguished from the experimental data.

should only be used as a qualitative measure of stacking, the data indicate that 2-aminopurine is more strongly stacked in HP2 than in HP1.

A clear difference between HP1 and HP2 is also reflected upon addition of Mg^{2+} or Ca^{2+} ions. In the case of HP1, addition of these ions leads to an increase of the fluorescence (Figure 2), whereas an overall decrease is observed for HP2 (Figure 3). In both cases the titration data cannot be described by binding of the ions to a single binding site. The existence of (at least) two types of binding sites in HP2 is reflected by an initial decrease followed by an increase of the fluorescence intensity upon ion addition. Binding to both sites in HP1 is accompanied by an increase of fluorescence. Least-squares fitting of the data, assuming binding to independent sites, leads to binding constants in the range of 700 M^{-1} and 40 M^{-1} for the first and the second binding process, respectively, for both HP1 and HP2 (buffer B, Table 1). The binding constants and the fluorescence changes for Mg^{2+} and Ca^{2+} are equivalent within the limits of accuracy. Binding constants in buffer T are higher than those in buffer B because of the lower ionic strength of buffer T (Table 1).

Temperature-Jump Measurements. Detection of fast relaxation processes requires an indication system that is at least as fast as the process to be characterized. In the present investigation we used the fluorescence of 2-aminopurine to analyze conformational transitions in the RNA hairpin loop. This indication is based on the strong dependence of the fluorescence intensity of 2-aminopurine on its degree of stacking. Thus, it first has to be established that stacking of 2-aminopurine is a fast process. For this purpose we used a single-stranded dodecariboadenylate with a 2-aminopurine substitution at position 8 [2AP-oligo(A)]. Stacking in single-stranded oligo- and polyriboadenylates is known to be associated with relaxation time constants < 1 μs (*29*−*32*). Measurements of the fluorescence-detected temperature-jump relaxation of 2AP-oligo(A) showed a fast relaxation process, partly reflecting the physical process of thermal quenching: the time constant corresponds to the "machine time", determined by the heating time constant and the response time constant of the optical detection system. Thus, the stacking relaxation in 2AP-oligo(A), reported by the fluorescence of 2-aminopurine, is faster than ∼1 μs.

Temperature-jump experiments on solutions of HP1 show a continuous decrease of the fluorescence in the microsecond time range (Figure 4): a first process with a time constant below the time resolution reflects (mainly) the physical process of thermal quenching; a second process is associated with a time constant of 22.1 μs, clearly reflecting chemical relaxation and indicating a change of the loop conformation. Because the relaxation effect is observed in the temperature range around 10 °C, very far below the thermal helix−coil transition at 67 °C, it cannot be assigned to a process contributing to this transition.

Corresponding temperature-jump experiments on solutions of HP2 show a very different relaxation response (Figure 5): in the first part of the relaxation curve the fluorescence decreases, whereas in a second part an increase of the fluorescence is observed. A least-squares fit of this relaxation

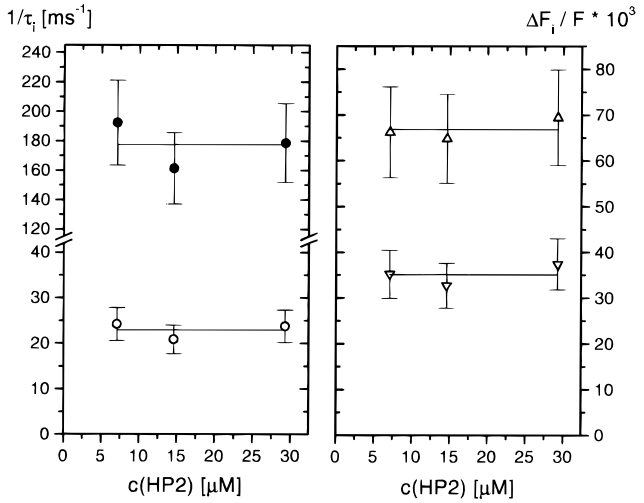

FIGURE 6: Reciprocal relaxation time constants $1/\tau_1$ (●) and $1/\tau_2$ (○) and relative amplitudes $\Delta F/F_1$ (Δ) and $\Delta F/F_2$ (▽) of HP2 observed for temperature jumps from 2 to 8.1 °C as a function of the HP2 concentration in buffer B. The lines represent average values.

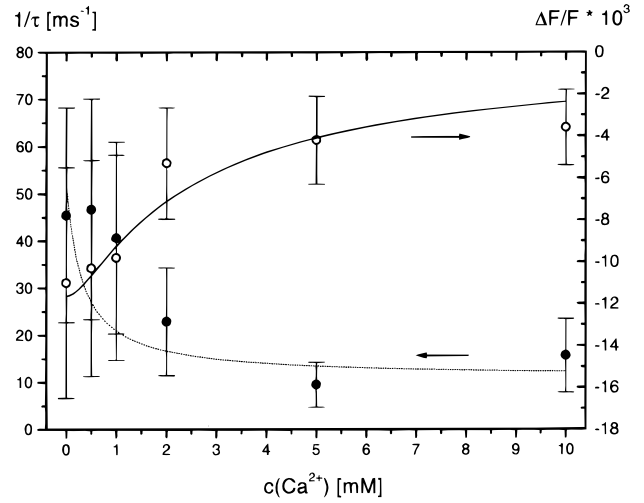

FIGURE 7: Reciprocal relaxation time constants $1/\tau$ (●) and relative amplitudes $\Delta F/F$ (○) of HP1 observed for temperature jumps from 2 to 8.1 °C as a function of the Ca^{2+} concentration in buffer B. The lines represent a fit of the combined data to the reaction model I (cf. text) with the parameters given in Table 2 together with the relative quantum yield $\alpha = 0.45$ and $\beta = 1.93$ (from equilibrium titrations and application of eqs 2 and 3) and the changes of the equilibrium constants $\Delta \ln K_1' = -0.036$ (fitted parameter) and $\Delta \ln K_2' = 0$ (fixed parameter).

curve demonstrates the existence of two relaxation processes in addition to an unresolved fast one, which is mainly due to the usual physical process of thermal quenching. The two resolved relaxation processes with time constants $\tau^c_1 = 5.2$ μs and $\tau^c_2 = 41.3$ μs indicate changes of conformation and are both associated with an increase of fluorescence. These data demonstrate that there are (at least) three states of the conformation of HP2, whereas only two states are indicated by the relaxation of HP1. As a test for interactions between RNA molecules, we measured the hairpin relaxation as a function of the hairpin concentration. The time constants and the amplitudes observed for HP2 are independent of the RNA concentration within experimental accuracy (Figure 6) and, thus, demonstrate that the conformational change is intramolecular.

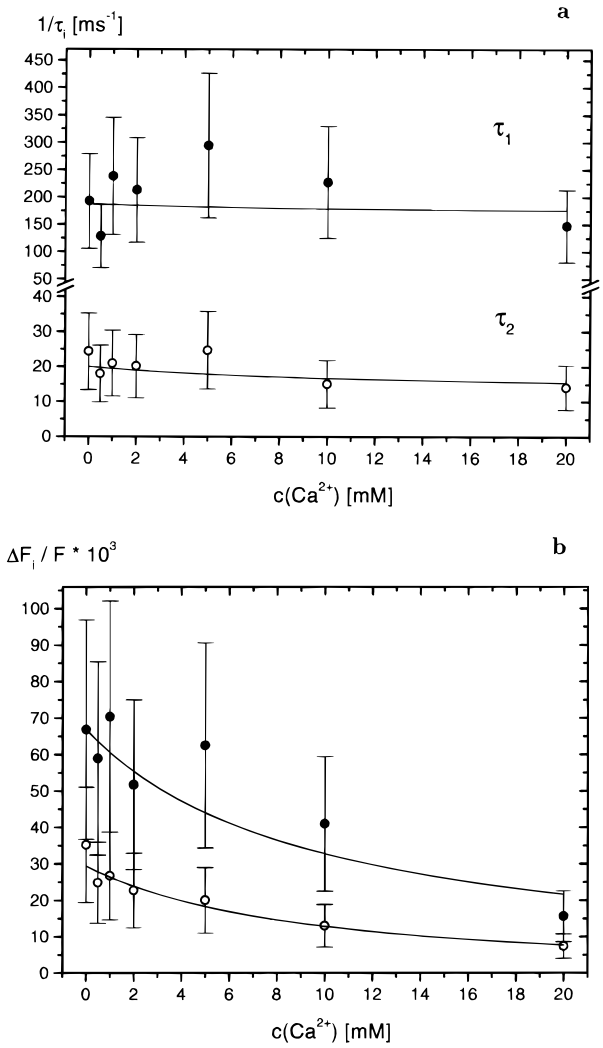

FIGURE 8: (a) Reciprocal relaxation time constants $1/\tau_1$ (●) and $1/\tau_2$ (○) and (b) relative amplitudes $\Delta F/F_1$ (●) and $\Delta F/F_2$ (○) of HP2 observed for temperature jumps from 2 to 8.1 °C as a function of the Ca^{2+} concentration in buffer B. The lines represent a fit of the combined data to the reaction model II (cf. text) with the parameters given in Table 3 together with the relative quantum yields $\alpha = 2.0$, $\beta = 0.98$, and $\gamma = 0.34$ (from equilibrium titrations and application of eqs 5 and 6) and the changes of the equilibrium constants $\Delta \ln K_1'' = -1.04$ (fitted parameter), $\Delta \ln K_2'' = -0.035$ (fitted parameter), and $\Delta \ln K_3'' = 0$ (fixed parameter).

More information on the intramolecular transition may be obtained by coupling of this transition to some ligand binding reaction. In the case of RNA hairpins, a ligand of interest is Mg^{2+}, because it is required for most biological functions of RNA and is expected to shift the conformational equilibrium. We compared the influence of Mg^{2+} and of Ca^{2+} ions to test for the potential formation of inner-sphere complexes (*33*, *34*), which should be reflected by a specific slow relaxation process in the case of Mg^{2+}. Addition of both Mg^{2+} and Ca^{2+} ions to HP1 leads to a decrease of the fluorescence amplitude and also a decrease of the reciprocal time constant (Figure 7). Any additional relaxation effect in the presence of Mg^{2+} was not observed and, thus, there is no evidence for the existence of inner-sphere complexes.

The change of the relaxation time constants for HP2 upon addition of Mg^{2+} or Ca^{2+} is small and remains within the limits of experimental accuracy, whereas the amplitudes are clearly reduced by addition of Mg^{2+} and Ca^{2+} (Figure 8).

Again addition of Mg^{2+} did not induce the appearance of any specific relaxation effect and, thus, no inner-sphere complexes seem to be formed.

Model Analysis of Relaxation Data. The hairpin RNA molecules used in the present investigation contain 15 nucleosides and 14 phosphates. Thus, according to simple stoichiometry of charges, up to 7 bivalent ions may bind to these hairpins. The equilibrium titrations described above revealed binding parameters for two binding processes of Mg^{2+}. The conformational relaxation observed in the absence of bivalent ions revealed the existence of two states in the case of HP1 and of three states in the case of HP2. Combination of all the known or expected reactions leads to complex reaction schemes with large numbers of parameters, which cannot be determined from the available experimental data. Thus, it is necessary to simplify the reaction schemes considerably.

The single relaxation process of HP1 is affected by binding of bivalent ions. A minimal reaction scheme for description of these data includes an intramolecular conformation change

$$A \underset{k'_{21}}{\overset{k'_{12}}{\rightleftharpoons}} B \tag{1a}$$

coupled with binding of bivalent ions to one of these states

$$B + Me^{2+} \underset{k'_{32}}{\overset{K'_{23}}{\rightleftharpoons}} C \tag{1b}$$

It is expected that bivalent ions bind to both states. However, the data suggest that binding occurs preferentially to one of the states. Because the available data do not provide enough information for a detailed description of differential ion binding to states A and B, binding to one of the states is neglected in a first approximation. We used the (first) equilibrium binding constant (K_1) together with the fluorescence quenching (q_1) derived from the titration curves (Table 1) for data fitting. The overall binding constant K determined by equilibrium titrations is related to the individual binding constants $K'_1 = k'_{12}/k'_{21}$ and $K'_2 = k'_{23}/k'_{32}$ by

$$K = \left(\frac{K'_1}{K'_1 + 1}\right) K'_2 \tag{2}$$

The relative fluorescence change Δ obtained from titrations [Δ = (fluorescence intensity in the limit of saturation with Me^{2+})/(fluorescence intensity before addition of Me^{2+})] is related to the individual quantum yields by

$$\frac{1}{\Delta} = \left(\frac{1}{K'_1 + 1}\right)\alpha + \left(\frac{K'_1}{K'_1 + 1}\right)\beta \tag{3}$$

where α and β are the quantum yields of A and B relative to that of C, respectively. The ion binding was assumed to be diffusion-controlled, as should be expected in the absence of inner-sphere complexation (*33*, *34*). A sample fit of experimental data to this model using the binding constant for the high-affinity site determined by equilibrium titrations is shown in Figure 7. The resulting parameters (Table 2) show that one of the loop conformations (A) is preferred in absence of bivalent ions; binding of bivalent ions induces a shift to the other loop conformation (B). The rate constants of the conformational transition are in the range of 10^4 s^{-1}.

Table 2: Kinetic and Thermodynamic Parameters for the Transition of HP1 in the Presence of Ca^{2+} or Mg^{2+}: Definition of the Mechanism and of the Parameters in Eq 1[a]

T (°C)	8.1	8.1	10.6
metal ion	Ca^{2+}	Mg^{2+}	Mg^{2+}
K'_1	0.27	0.27	0.46
k'_{12} (s^{-1})	$1.1 \cdot 10^4$	$1.1 \cdot 10^4$	$2.3 \cdot 10^4$
k'_{21} (s^{-1})	$4.2 \cdot 10^4$	$4.0 \cdot 10^4$	$5.1 \cdot 10^4$
K'_2 (M^{-1})	3100	3900	2600
k'_{23} (M^{-1} s^{-1})	$1.0 \cdot 10^{10}$	$1.0 \cdot 10^{10}$	$1.0 \cdot 10^{10}$
k'_{32} (s^{-1})	$3.2 \cdot 10^6$	$2.6 \cdot 10^6$	$3.8 \cdot 10^6$
K (M^{-1})	660	820	820

[a] The parameters are given at the final temperatures T of the jump experiments; estimated accuracy ±20%; buffer B. The overall binding constants K are from equilibrium titrations; the rate constants k'_{23} are assumed to be diffusion-controlled, because there is no evidence for inner sphere complexation. All the other parameters were obtained by fitting of the experimental data.

The data obtained for Mg^{2+} and Ca^{2+} are identical within experimental accuracy.

A quantitative description of the data obtained for HP2 is more difficult, because there are three conformational states already in the absence of bivalent ions:

$$A \underset{k''_{21}}{\overset{k''_{12}}{\rightleftharpoons}} B \underset{k''_{32}}{\overset{k''_{23}}{\rightleftharpoons}} C \tag{4a}$$

Again the experimental data indicate that one of the states is favored by binding of bivalent ions. Because the available information is not sufficient to describe differential ion binding to the three states, we use a scheme with ion binding to only one of the states:

$$B + Me^{2+} \underset{k''_{43}}{\overset{k''_{34}}{\rightleftharpoons}} D \tag{4b}$$

The overall binding constant K determined by equilibrium titrations is related to the individual binding constants $K''_1 = k''_{12}/k''_{21}$, $K''_2 = k''_{23}/k''_{32}$, and $K''_3 = k''_{34}/k''_{43}$ by

$$K = \left(\frac{K''_1}{K''_1 K''_2 + K''_1 + 1}\right) K''_3 \tag{5}$$

The relative fluorescence change Δ obtained from titrations (definition as given above) is related to the individual quantum yields by

$$\frac{1}{\Delta} = \left(\frac{1}{K''_1 K''_2 + K''_1 + 1}\right)\alpha + \left(\frac{K''_1}{K''_1 K''_2 + K''_1 + 1}\right)\beta + \left(\frac{K''_1 K''_2}{K''_1 K''_2 + K''_1 + 1}\right)\gamma \tag{6}$$

where α, β, and γ are the respective quantum yields of A, B, and C relative to that of D. With this simplified reaction scheme the experimental data were fitted at a reasonable accuracy (cf. Figure 8) with the binding constant for the low-affinity site (K_2) together with the fluorescence quenching (q_2) determined by equilibrium titrations (Table 1). Satisfactory fits were not obtained with the binding constant for the high-affinity site (K_1). The parameters obtained from these fits (Table 3) are again identical for Mg^{2+} and Ca^{2+} within experimental accuracy.

Table 3: Kinetic and Thermodynamic Parameters for the Transition of HP2 in the Presence of Ca^{2+} or Mg^{2+}: Definition of the Mechanism and of the Parameters in Eq 4[a]

T (°C)	8.1	8.1	10.6	10.6
metal ion	Ca^{2+}	Mg^{2+}	Ca^{2+}	Mg^{2+}
K_1''	10	10	10	10
k_{12}'' (s^{-1})	$1.7 \cdot 10^5$	$2.0 \cdot 10^5$	$2.0 \cdot 10^5$	$2.0 \cdot 10^5$
k_{21}'' (s^{-1})	$1.7 \cdot 10^4$	$2.0 \cdot 10^4$	$2.0 \cdot 10^4$	$2.0 \cdot 10^4$
K_2''	0.60	0.60	0.60	0.65
k_{23}'' (s^{-1})	$7.8 \cdot 10^3$	$9.4 \cdot 10^3$	$1.1 \cdot 10^4$	$1.3 \cdot 10^4$
k_{32}'' (s^{-1})	$1.3 \cdot 10^4$	$1.5 \cdot 10^4$	$1.9 \cdot 10^4$	$2.1 \cdot 10^4$
K_3'' (M^{-1})	100	93	100	93
k_{34}'' ($M^{-1}\,s^{-1}$)	$1.0 \cdot 10^{10}$	$1.0 \cdot 10^{10}$	$1.0 \cdot 10^{10}$	$1.0 \cdot 10^{10}$
k_{43}'' (s^{-1})	$9.8 \cdot 10^7$	$1.1 \cdot 10^8$	$9.8 \cdot 10^7$	$1.1 \cdot 10^8$
K (M^{-1})	36	53	36	53

[a] The parameters are given at the final temperatures T of the jump experiments; estimated accuracy ±40%; buffer B. The overall binding constants K are from equilibrium titrations; the rate constants k_{34}'' are assumed to be diffusion-controlled, because there is no evidence for inner sphere complexation. All the other parameters were obtained by fitting of the experimental data.

The results obtained by fitting of the relaxation data are presented here to demonstrate an interpretation in terms of the simplest mechanisms that are consistent with these data. As usual in kinetics, we cannot exclude more complex mechanisms. We also note that the parameters represent a first approximation and that the accuracy should be improved by future more extensive investigations, including the temperature dependence, for example.

DISCUSSION

RNA loops have been favored objects of investigations during recent years. Structures of various RNA loops were determined by X-ray or NMR analysis. In all cases a well-defined structure was found. The structure of the GAAA tetraloop was determined in a model hairpin RNA by NMR (*7*) and within both a hammerhead ribozyme (*8*) and a group I ribozyme (*10*, *11*) by X-ray analysis. In addition, the structures of the GCAA and GAGA loops were determined by NMR analysis (*7*) and that of the GUAA loop in a hammerhead ribozyme (*9*). Wedekind and McKay (*35*) state that the "structures superimpose remarkably well considering the variety of environments and conditions under which they have been characterized". Thus, the present evidence for the existence of more than a single conformation for a GNRA tetraloop appears to be in contradiction with the literature. However, the GCGA tetraloop structure in domain E of *Thermus flavus* 5S RNA determined by X-ray analysis is "in distinctly different conformation from other GNRA tetraloops analyzed by NMR" (*12*).

Chemical relaxation shows directly the number of reaction states in solution. However, the precise characterization of the nature of these states is much more difficult. Some information derives from the relaxation time constant: the transition between the states is slow relative to base stacking in single-stranded oligo- and polyribonucleotides (*29*−*32*). The relaxation time constants of stacking in single-stranded oligoriboadenylates were found in the time range below 1 μs. The relatively low rate of the transition in the tetraloop determined here indicates that the conformational transition does not correspond to a "simple" stacking reaction. It is likely that the loop transition involves a stacking rearrangement of more than a single residue. Probably the reaction rate is slowed by steric constraints imposed by the loop structure.

A similar transition with a relaxation time constant of ~100 μs has been observed in the anticodon loop of $tRNA^{Phe}$ by the fluorescence of the wye-base. This transition was found in the complete $tRNA^{Phe}$ and also in the isolated anticodon loop, whereas a hexamer, excised from the anticodon loop including the wye-base but without loop structure, no longer showed the transition (*36*, *37*). Thus, the loop structure of the anticodon loop is essential for the transition, which has been assigned tentatively to a conversion between a 3′-stack and a 5′-stack conformation (Figure 9).

In the present case the loop transition was monitored by the fluorescence of 2-aminopurine residues. 2-Aminopurine is not expected to induce any major change in the structure or in the transition. This view is supported by experiments on a hairpin loop with the sequence used in the present investigation but without 2-aminopurine substitution: a relaxation effect characteristic of the loop structure is also detected by measurements of UV absorbance (Porschke, unpublished observations).

Some information on the structure of the loop and its transition may be obtained from the fluorescence of the 2-aminopurine residues: the fluorescence of 2-aminopurine in HP2 is quenched much more than that in HP1, indicating that 2-aminopurine in the third position (L3) of the loop is more strongly stacked than that in the second position (L2). This result is consistent with the standard structure of the tetraloop determined by NMR and X-ray analysis (*7*, *35*). It corresponds to a preference of the 3′-stack conformation (Figure 9a). A preferential 3′-stack conformation is also consistent with the following simple interpretation of the number of the observed relaxation processes: in the hairpin HP2, 2-aminopurine is in loop position L3 and thus reports both its own stacking toward the 3′-end and stacking of the adjacent base in position L2, resulting in two relaxation processes; in hairpin HP1 2-aminopurine is in position L2 and thus does not directly report stacking of the base in position L3 toward the 3′-end but directly reports its own stacking on top of the base in position L3, resulting in one relaxation process with detectable amplitude. In general, both reactions should be reported by indicators in the two different positions due to mutual coupling of the reactions. Nevertheless, amplitudes are expected to be particularly large when an indicator is directly involved in a reaction.

The direction of the fluorescence change observed upon addition of bivalent ions may also be used for an assignment. Addition of bivalent ions to HP1 leads to an increase of the fluorescence, suggesting some reduction of stacking in the second position of the loop. This is consistent with a transition in the direction from a 5′- to 3′-stack (Figure 9, d → a), because the degree of stacking of the second residue is expected to be lower in a 3′-stack than in a 5′-stack. In HP2 addition of bivalent ions leads to a decrease of fluorescence, indicating enhanced stacking in the third position of the loop, which is again consistent with a transition from a 5′- to a 3′-stack. Obviously, these arguments should be used with caution because changes of fluorescence intensity may also be influenced by other factors. Thus, we do not have sufficient evidence for an assignment of given loop structures to the states revealed by relaxation analysis.

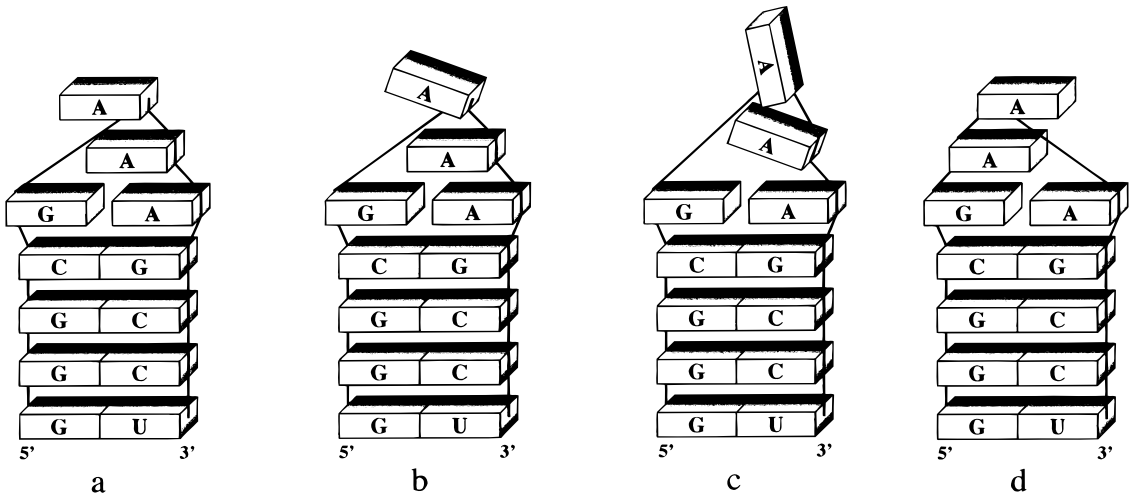

FIGURE 9: Schematic models of hairpin loop structures, shown for the loop sequence GAAA; loop residues L1 and L4 form the unusual G−A base pair. (a) 3′-stacked conformation with full stacking; (b) 3′-stack with unstacked residue L2; (c) conformation with unstacked residues L2 and L3; (d) 5′-stacked conformation with full stacking.

Our data indicate that the states observed for the hairpin loops coexist in similar concentrations under the conditions of our temperature-jump experiments.

The fast component of the fluorescence change induced by temperature jumps corresponds to quenching for both hairpin loops and is consistent with standard thermal quenching. However, the "chemical" relaxation amplitudes are in opposite directions: a decrease of fluorescence is observed for HP1, whereas an increase is found for both relaxation effects of HP2. These amplitudes suggest an increase of 2-aminopurine stacking with increasing temperature for HP1 and a corresponding decrease for HP2. Thus, the amplitudes again support the interpretation of the observed effects in terms of a stacking rearrangement. The direction of the fluorescence change suggests that increasing temperature favors a 5′-stack. In all cases the fluorescence changes observed for HP1 and HP2 were found to be correlated: a given change reported by 2-aminopurine for the second loop position (HP1) is associated with the opposite change reported by 2-aminopurine in the third loop position (HP2).

The relatively low rate of the conformational transition in the tetraloop suggests that this transition is slowed by the presence of unusual structure elements in the loop, e.g., the G−A base pair, a hydrogen bond between a G-base and a phosphate, or the occurrence of ribose in the 2′-endo conformation. An unusual base pair or ribose in the 2′-endo conformation was not found in the anticodon loop of $tRNA^{Phe}$, whereas a hydrogen bond between a base (U_{33}) and a phosphate is also formed in the anticodon loop. However, it is not likely that this type of hydrogen bond is essential for the slow transition. Heus and Pardi (*5*) mention that the sugars of the middle two nucleotides of the tetraloop are "averages" of 2′-endo and 3′-endo forms. According to the NMR results, these residues appear to be the only parts of the structure displaying a conformational equilibrium. It would be remarkable if these transitions are essential for the relatively slow process detected in the present investigation, because simulations indicate that the 2′-endo to 3′-endo transition is a very fast reaction (*38*−*40*). However, it cannot be excluded that coupling of ring pucker transitions with rearrangements of base stacking results in a relatively slow reaction. For the case of the CUUG loop, Jucker and Pardi (*6*) reported that residues in the loop "were undergoing motions in the intermediate to fast exchange time scale" and Reif et al. (*41*) found for the same loop with 2′-fluoro substitutions "two distinct conformations that differ in the sugar conformation". At present an unequivocal assignment of the different loop conformations is not possible yet. This should become possible by using a combination of methods, including computer simulations, NMR measurements, and relaxation measurements, on loops of various sequences.

ACKNOWLEDGMENT

We thank T. Tuschl for helpful discussions in the initial phase of this study.

REFERENCES

1. Varani, G. (1995) *Annu. Rev. Biophys. Biomol. Struct. 24*, 379−404.
2. Westhof, E., Romby, P., Romaniuk, P. J., Ebel, J. P., Ehresmann, C., and Ehresmann, B. (1989) *J. Mol. Biol. 207*, 417−431.
3. de Stevenson, I. L., Romby, P., Baudin, F., Brunel, C., Westhof, E., Ehresmann, C., Ehresmann, B., and Romaniuk, P. J. (1991) *J. Mol. Biol. 219*, 243−255.
4. Cheong, C., Varani, G., and Tinoco, I., Jr. (1990) *Nature 346*, 680−682.
5. Heus, H. A., and Pardi, A. (1991) *Science 253*, 191−194.
6. Jucker, F. M., and Pardi, A. (1995) *Biochemistry 34*, 14416−14427.
7. Jucker, F. M., Heus, H. A., Yip, P. F., Moors, E. H. M., and Pardi, A. (1996) *J. Mol. Biol. 264*, 968−980.
8. Pley, H., Flaherty, K. M., and McKay, D. B. (1994) *Nature 372*, 111−113.
9. Scott, W. G., Finch, J. T., and Klug, A. (1995) *Cell 81*, 991−1002.
10. Cate, J. H., Gooding, A. R., Podell, E., Zhou, K., Golden, B. L., Kundrot, C. E., Cech, T. R., and Doudna, J. A. (1996) *Science 273*, 1678−1685.
11. Cate, J. H., Gooding, A. R., Podell, E., Zhou, K., Golden, B. L., Szewczak, A. A., Kundrot, C. E., Cech, T. R., and Doudna, J. A. (1996) *Science 273*, 1696−1699.
12. Perbandt, M., Nolte, A., Lorenz, S., Bald, R., Betzel, C., and Erdmann, V. A. (1998) *FEBS Lett. 429*, 211−215.
13. Leulliot, N., Baumruk, V., Abdelkafi, M., Turpin, P. Y., Namane, A., Gouyette, C., Huynh-Dinh, T., and Ghomi, M. (1999) *Nucleic Acids Res. 27*, 1398−1404.

14. Meroueh, M., and Chow, C. S. (1999) *Nucleic Acids Res. 27*, 1118−1125.
15. Williams, D. J., and Hall, K. B. (1999) *Biophys. J. 76*, 3192−3205.
16. Akke, M., Fiala, R., Jiang, F., Patel, D., and Palmer, A. G. (1997) *RNA 3*, 702−709.
17. Kirchner, R., Vogtherr, M., Limmer, S., and Sprinzl, M. (1998) *Antisense Nucleic Acid Drug Dev. 8*, 507−516.
18. Shubsda, M., Goodisman, J., and Dabrowiak, J. C. (1999) *Biophys. Chem. 76*, 95−115.
19. Tuschl, T., Ng, M. M. P., Pieken, W., Benseler, F., and Eckstein, F. (1993) *Biochemistry 32*, 11658−11668.
20. Menger, M., Tuschl, T., Eckstein, F., and Porschke, D. (1996) *Biochemistry 35*, 14710−14716.
21. Porschke, D., and Jung, M. (1982) *Nucleic Acids Res. 10*, 6163−6176.
22. Rigler, R., Rabl, C. R., and Jovin, T. M. (1974) *Rev. Sci. Instrum. 45*, 580−588.
23. Porschke, D., and Jung, M. (1985) *J. Biomol. Struct. Dyn. 2*, 1173−1184.
24. Diekmann, S., Hillen, W., Morgeneyer, B., Wells, R. D., and Porschke, D. (1982) *Biophys. Chem. 15*, 263−270.
25. Avery, L. (1982) *J. Chem. Phys. 76*, 3242−3248.
26. Ilgenfritz, G. (1977) *Mol. Biol. Biochem. Biophys. 24*, 1−42.
27. Ward, D. C., Reich, E., and Stryer, L. (1969) *J. Biol. Chem. 244*, 1228−1237.
28. Kelley, S. O., and Barton, J. K. (1999) *Science 283*, 375−381.
29. Porschke, D. (1973) *Eur. J. Biochem. 39*, 117−126.
30. Porschke, D. (1977) *Mol. Biol. Biochem. Biophys. 24*, 191−218.
31. Porschke, D. (1978) *Biopolymers 17*, 315−323.
32. Dewey, T. G., and Turner, D. H. (1979) *Biochemistry 18*, 5757−5762.
33. Diebler, H., Eigen, M., Ilgenfritz, G., Maass, G., and Winkler, R. (1969) *Pure Appl. Chem. 20*, 93−115.
34. Porschke, D. (1995) in *The Biological chemistry of magnesium* (Cowan, J. A., Ed.) VCH Publishers, New York.
35. Wedekind, J. E., and McKay, D. B. (1998) *Annu. Rev. Biophys. Biomol. Struct. 27*, 475−502.
36. Labuda, D., and Porschke, D. (1982) *Biochemistry 21*, 49−53.
37. Bujalowski, W., Graeser, E., McLaughlin, L. W., and Porschke, D. (1986) *Biochemistry 25*, 6365−6371.
38. Nowakowski, J., Miller, J. L., Kollman, P. A., and Tinoco, I., Jr. (1996) *J. Am. Chem. Soc. 118*, 12812−12820.
39. Hermann, T., Auffinger, P., and Westhof, E. (1998) *Eur. Biophys. J. 27*, 153−165.
40. Petrova, P., Koca, J., and Imberty, A. (1999) *J. Am. Chem. Soc. 121*, 5535−5547.
41. Reif, B., Wittmann, V., Schwalbe, H., Griesinger, C., Wörner, K., Jahn-Hofmann, K., and Engels, J. W. (1997) *Helv. Chim. Acta 80*, 1952−1971.

BI992297N